RZ 3882 (#ZUR1405-087) 05/30/2014
Physical Sciences 8 pages

Research Report

Image Distortions of a Partially Fluorinated Hydrocarbon Molecule in Atomic Force Microscopy with Carbon Monoxide Terminated Tips

Nikolaj Moll,[1] Bruno Schuler,[1] Shigeki Kawai,[2] Feng Xu,[3] Lifen Peng,[3] Akihiro Orita,[3] Junzo Otera,[3] Alessandro Curioni,[1] Mathias Neu,[4] Jascha Repp,[4] Gerhard Meyer,[1] and Leo Gross[1]

[1]IBM Research – Zurich, 8803 Rüschlikon, Switzerland
[2]Department of Physics, University of Basel, 4056 Basel, Switzerland, and PRESTO, Japan Science and Technology Agency, 4056 Basel, Switzerland
[3]Department of Applied Chemistry, Okayama University of Science, 1-1 Ridai-cho, Kita-ku, Okayama, 700-0005, Japan
[4]Institute of Experimental and Applied Physics, University of Regensburg, 93053 Regensburg, Germany

Image distortions of a partially fluorinated hydrocarbon molecule in atomic force microscopy with carbon monoxide terminated tips

Nikolaj Moll,[*,†] Bruno Schuler,[†] Shigeki Kawai,[‡] Feng Xu,[¶] Lifen Peng,[¶] Akihiro Orita,[¶] Junzo Otera,[¶] Alessandro Curioni,[†] Mathias Neu,[§] Jascha Repp,[§] Gerhard Meyer,[†] and Leo Gross[†]

IBM Research – Zurich, Säumerstrasse 4, 8803 Rüschlikon, Switzerland, Department of Physics, University of Basel, Klingbergstrasse 82, 4056 Basel, Switzerland, and PRESTO, Japan Science and Technology Agency, Klingelbergstrasse 82, 4056 Basel, Switzerland, Department of Applied Chemistry, Okayama University of Science, 1-1 Ridai-cho, Kita-ku, Okayama, 700-0005, Japan, and Institute of Experimental and Applied Physics, University of Regensburg, 93053 Regensburg, Germany

E-mail: nim@zurich.ibm.com

Abstract

The underlying mechanisms of image distortions in atomic force microscopy (AFM) with CO-terminated tips are identified and studied in detail. AFM measurements of a partially fluorinated hydrocarbon molecule recorded with a CO-terminated tip are compared with state-of-the-art *ab initio* calculations. The hydrogenated and fluorinated carbon rings in the molecule appear different in size, which primarily originates from the different extents of their π-electrons. Further, tilting of the CO at the tip, induced by van der Waals forces, enlarges the apparent size of parts of the molecule by up to 50 %. Moreover, the CO tilting in response to local Pauli repulsion causes a significant sharpening of the molecule bonds in AFM imaging.

Keywords

single molecule, NC-AFM

Atomic resolution of molecules has recently been achieved with noncontact atomic force microscopy (AFM) using CO-terminated tips.[1–10] Images obtained with CO-terminated tips appear distorted,[1–4] which can be exploited to distinguish the bond order of individual carbon-carbon bonds in polycyclic aromatic hydrocarbons and fullerenes.[6] Here, we study this distortion resulting in an enlarged and sharpened appearance of the imaged molecules in more detail and identify the underlying mechanisms. For this, we imaged 4- (4-(2,3,4,5,6- pentafluorophenylethynyl)- 2,3,5,6-tetrafluorophenylethynyl) phenylethynylbenzene (FFPB)[11,12] [see Fig. 1(a)] atomically resolved with noncontact AFM as shown in Fig. 1(b). In FFPB, four carbon rings are con-

*To whom correspondence should be addressed

†IBM Research – Zurich, Säumerstrasse 4, 8803 Rüschlikon, Switzerland

‡Department of Physics, University of Basel, Klingbergstrasse 82, 4056 Basel, Switzerland, and PRESTO, Japan Science and Technology Agency, Klingelbergstrasse 82, 4056 Basel, Switzerland

¶Department of Applied Chemistry, Okayama University of Science, 1-1 Ridai-cho, Kita-ku, Okayama, 700-0005, Japan

§Institute of Experimental and Applied Physics, University of Regensburg, 93053 Regensburg, Germany

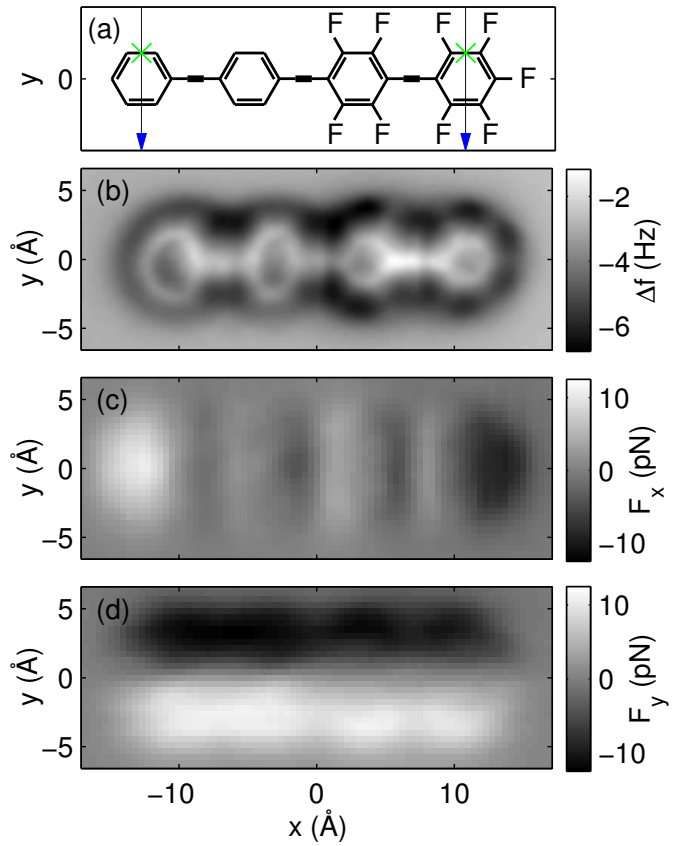

Figure 1: (a) The chemical structure of the FFPB molecule. Green crosses indicate the lateral positions y_{bond} which are compared to quantify the distortions, and blue arrows indicate the lateral positions of the linescans. (b) Measured constant-height frequency shift Δf image. The lateral forces extracted from a three dimensional force map: (c) F_x in the x-direction and (d) F_y in the y-direction. Measurements (b)−(d) correspond to a tip height of $z = 3.55$ Å.

nected by ethynylene units with triple bonds, with two rings being H-terminated and two rings F-terminated. In the following the rings are denoted as H-rings and F-rings, respectively. The FFPB molecules were deposited on a two-monolayer thick (100) NaCl film on Cu(111) [NaCl(2ML)/Cu(111)].

The adsorption geometry of the FFPB molecule on a bilayer NaCl film on Cu(100) was calculated with density functional theory (DFT).[13] The Cu(100) surface was used for the calculations because NaCl is commensurate for this surface orientation, leading to small super cells. A code with numerical atomic orbitals as basis functions[14] and the Perdew-Burke-Ernzerhof exchange-correlation functional (PBE)[15] was applied. A van der Waals method[16] combined with the Lifshitz-Zaremba-Kohn theory for the nonlocal Coulomb screening within the bulk for the Cu substrate[17] and calculated coefficients for *atoms in the solid*[18] for the NaCl film were used.

We found that in the calculations the FFPB molecule adsorbs with its long axis along a row of Na atoms in the [011] direction and that the four carbon rings have four different adsorption heights. For the orientation shown in Fig. 1(a), the vertical positions z of the C atoms of the planar rings are, from left to right: 0.00 Å, −0.06 Å, 0.01 Å, and 0.09 Å. The left H-ring is our reference and defines zero for the vertical position z. The outer F-ring relaxes 0.09 Å further away from the substrate than the outer H-ring.

The AFM measurements were performed with a combined STM/AFM using a qPlus sensor[19] operated in frequency-modulation mode[20] under ultrahigh vacuum and low temperature of 5 K. As substrate, we used two-monolayer thick (100)-oriented NaCl islands grown on Cu. FFPB molecules were thermally evaporated on the sample at 10 K and low coverages of CO molecules were co-adsorbed to terminate the tip with CO.[21] The AFM image of a single FFPB molecule is shown in Fig. 1(b) displaying the frequency shift Δf of the sensor's resonance with respect to its resonance frequency f_0 far away from the surface. Fig. 1(b) shows the frequency shift measured at constant height, parallel to the NaCl surface. Fig. 1(c)-(d) show the lateral forces extracted from a three-dimensional force map, obtained using $\Delta f(z)$ spectroscopy on a grid.[22]

To determine the orientation of the molecule we employed Kelvin probe force microscopy (KPFM). Here we used a Cu terminated tip, obtained by controlled contact of the tip with the Cu(111) surface. We recorded a map of the local contact potential difference (LCPD) of the FFPB molecule on NaCl(2ML)/Cu(111) using $\Delta f(V)$ spectroscopy at constant height,[12,23]

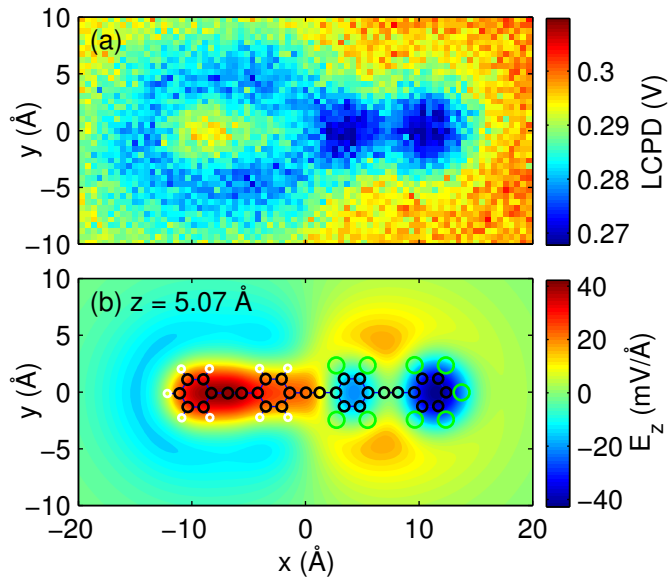

Figure 2: (a) The LCPD measured by KPFM using a Cu tip. (b) The z-component of the electric field E of the FFPB molecule at z = 5.07 Å.

shown in Fig. 2(a). The LCPD contrast can be qualitatively compared to the z component of the electrostatic field E,[23,24] which we calculated for the free FFPB molecule, shown in Fig. 2(b). The qualitatively different contrast obtained on the H- and F- terminated rings and the good qualitative agreement with the calculations provide us with the molecular orientation. Making use of this information obtained by KPFM we assigned the H-rings (left) and F-rings (right) in Fig. 1 and Fig. 2 as displayed in the model in Fig. 1(a). In Fig. 1(b) the H-rings appear with a larger diameter than the F-rings of the FFPB molecule. The halo, i.e., the region of minimal frequency shift surrounding the molecule, is less pronounced around the H-rings than around the F-rings.

We also determined the adsorption height and geometry of the FFPB molecule on the substrate using AFM.[9] We subtracted the background forces corresponding to the underlying substrate and used z^*, that is, the tip height at minimal frequency, as measure for the adsorption height. The FFPB molecule adsorbs along a row of Na surface atoms, in agreement with the calculations. We use the calculations (as described later) to calibrate the tip height and set the tip height with minimal frequency z^* at the center of the outer H-ring to z^* = 3.93 Å. Note that we subtracted the background forces corresponding to the underlying substrate for the experimental determination of z^*.[9] For the center of the outer F-ring, we measured z^* = 4.03 Å. In conclusion the AFM measurements yield that the outer F-ring relaxes outwards by 0.10 Å compared to the outer H-ring, which matches the calculated height difference of 0.09 Å very well. These results indicate that the adsorption geometry of the FFPB molecule on the substrate is very well described by the calculations with respect to the experiment. Differences in the adsorption height can lead to different apparent bond length and thus different apparent ring sizes as recently shown.[4] The similar adsorption heights of the different rings, which we found by experiment and theory, indicate that for the FFPB molecule this effect will be small and other reasons must be responsible for the smaller appearance of F-rings compared to H-rings.

Next, we computationally investigated the mechanisms for the distortion of the AFM images obtained with CO-functionalized tips. To calculate the frequency shift spectra, we removed the underlying substrate but kept the atomic positions of the FFPB molecule fixed. Otherwise, the computational time would be prohibitively long. We calculated the total energy of the FFPB molecule interacting with a vertical Cu-dimer tip functionalized with a CO.[6] We used the Cu-dimer as the metallic part of the tip in our calculations, because its spring constant of 0.49 N/m seems to be similar to that of the experiment,[25] it shows spherical symmetry, and the small number of atoms reduces the computational costs. To obtain the frequency shift we took the second derivative with respect to the z-direction. We found that the tip height with minimal frequency z^* is 3.93 Å for the center of the outer H-ring (used for the calibration of the tip height z^* in the experiment) and 4.05 Å for the center of the outer F-ring.

First, to quantify the larger appearance of the rings in the AFM images, we looked at the lateral position y_{bond} of the molecular bond indi-

Table 1: The lateral position of the molecular bond y_{bond} between the two outer C atoms of the H- and F-ring indicated by the green crosses in Fig. 1(a): from the *geometry*, from the electron *density*, from the computed Δf image with a *fixed* CO at the tip, from the computed Δf image with a *relaxed* CO at the tip and from Δf image from *experiment*, respectively. For comparison the relative difference with respect to the value from the geometry is given in %.

	H-ring		F-ring	
	y_{bond} (Å)	%	y_{bond} (Å)	%
geometry	1.21		1.21	
density	1.45	20	1.05	-13
fixed	1.37	13	1.13	-6
relaxed	1.58	30	1.40	16
experiment	1.84	52	1.11	-8

cated by the green crosses in Fig. 1(a) with respect to the long molecular axis, which defines $y = 0$. Using the atomic positions of the calculated geometry of the FFPB molecule, we find that the outer H-ring and the outer F-ring have almost identical sizes in the y-direction as seen in Table 1. The difference in size is less than 0.4 %.

Because the atomic contrast is a consequence of Pauli repulsion,[2] which is related to the charge density,[26] we examined the charge density of the FFPB molecule. Again we removed the substate and kept the position of the molecule fixed. The charge density at constant height $z = 3.61$ Å is shown in Fig. 3(a). The charge density above the H-rings is approximately a factor of two larger than that above the F-rings. The different saturations of the rings with either H or F atoms also lead to drastic differences in the apparent sizes of the rings in the charge density. This can be attributed to the larger electronegativity of the F atoms, which seems to influence the π-electrons of the FFPB molecule.[12] The lateral position y_{bond} is given in Table 1 when taking the maximum of the charge density as a measure for the bond location. The lateral position y_{bond} for the H-ring is significantly larger and the lateral position y_{bond} for the F-ring is significantly smaller with respect to the positions determined from the geometry.

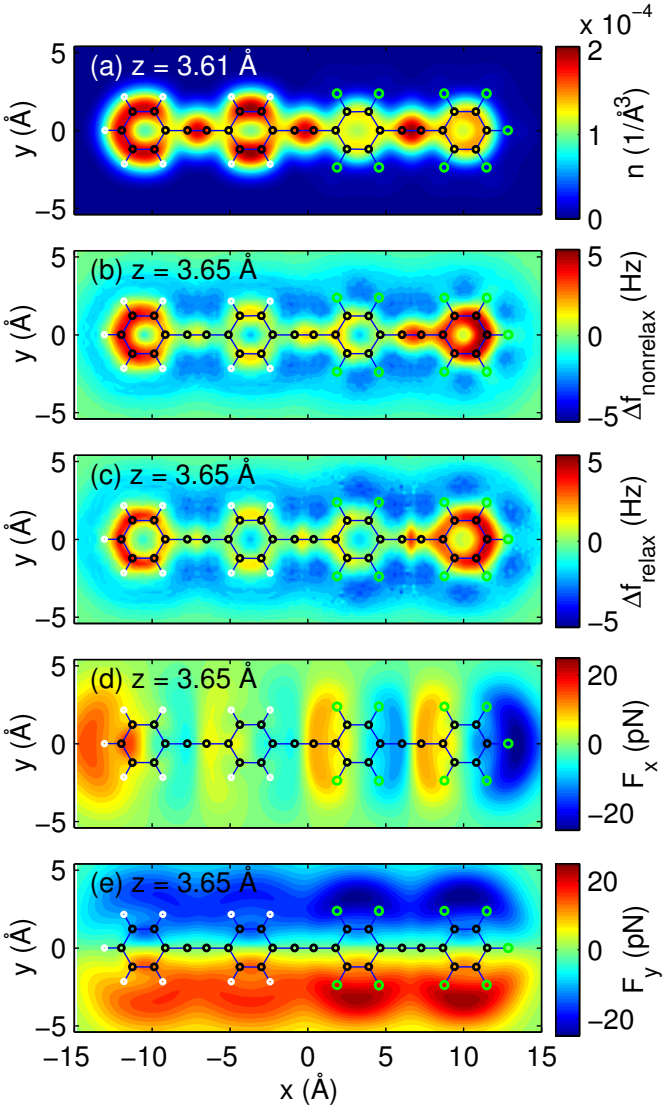

Figure 3: (a) The calculated charge density at a vertical position $z = 3.61$ Å and model of the FFPB molecule. (b) The calculated frequency shift Δf image at a tip height of $z = 3.65$ Å with a fixed CO at a Cu-dimer tip and (c) with CO relaxed at the tip. (d) The calculated force F_x in the x-direction and (e) F_y in the y-direction. The lateral forces always tilt the CO towards the center of the nearest ring of the FFPB molecule.

AFM images are calculated using a Cu-dimer tip functionalized with a CO. First we considered a fixed CO at the tip. All four tip atoms are confined along a line perpendicular to the sample surface. The distances of the atoms were relaxed for the isolated tip. The frequency

shift image is shown in Fig. 3(b). As in the experiment the halo around the F-rings is larger and more pronounced compared to the H-rings. The image resembles the charge density very closely, except for the fact that the outer H- and F-rings exhibit a larger positive frequency shift than to the two inner rings. In Table 1 the lateral position y_{bond} is given when taking the maximum of the frequency shift with this fixed tip as a measure. This value is relatively close to the corresponding value from the charge density for both the H-ring and the F-ring.

Next, the influence of the relaxation of the CO is examined. We calculated the frequency shift keeping the Cu-dimer tip fixed while relaxing the CO until the forces were smaller than 0.8 pN. The frequency shift image in Fig. 3(c) including relaxations of the CO shows some distinct differences to the image in Fig. 3(b) using a fixed CO. The halo around the F-rings is even more pronounced compared than that around the H-rings. Furthermore, all rings appear larger (Table 1). Tilting of the CO enlarges the apparent sizes of the H- and F-rings when comparing with the results with a fixed tip.

To understand the origin of the differences between experiment and computations, we determined the lateral forces experimentally and computationally. Experimentally, the lateral forces were obtained by integrating the frequency shift twice over the tip height to $z = 7.55$ Å and taking the lateral derivative in x- and y-directions.[27] However, as the tilt of the CO depends on the tip height, the lateral position of the probing O atom changes with the tip height. This will lead to an error in the integration.[3] The experimental lateral forces are shown in Fig. 1(c) and (d). The largest lateral forces arise above and in the vicinity (about 2 Å) of the molecule, corresponding to the extent of the halo around the molecule. The forces always point towards the center of the nearest ring. In Fig. 3(d) and (e) the computed lateral forces are shown, which were determined from the derivative in the corresponding lateral directions of the total energy of the FFPB molecule and tip system. The computed lateral forces are qualitatively very similar to the experimental ones. In the experiment, the lateral force F_y is similar in size above both types of rings, whereas in the computations it is larger above the F-rings than above the H-rings. The reason for the larger lateral force above the F-rings is not clear. The screening of the substrate which is neglected in our calculations might reduce the van der Waals contributions. Finally, electrostatic interactions might be another source of the remaining discrepancy between experiment and theory. Electrostatic interactions and their effect on the tilting are included in our theory, however, with some errors. The dipole moment of CO tips is not completely accurate in DFT and under debate experimentally.[28,29] Moreover, also higher order electrostatic multipole moments of the tip have to be taken into account.[24] The measured LCPD contrast and the calculated electrostatic field above the molecule (Fig. 2) are essentially inverted for H- with respect to F-rings. Therefore, electrostatic forces will act differently on H- and F-rings and could lead to different image distortions for both type of rings.

In the computations, we can examine the origin of the lateral forces in more detail. From the lateral displacement Δy of the O atom of the CO and the lateral force F_y, we can calculate an effective spring constant. This is 30 to 60 % larger than the inherent spring constant of 0.49 N/m for the tip calculated without a sample molecule.[6] The vertical force from the sample molecule acting on the CO leads to a additional restoring force. If we take a maximal vertical force of 80 pN and a lever arm of 3.02 Å,[25] this vertical force alone results an increase of the lateral spring constant of the CO molecule of 0.26 N/m.[3] Therefore, this additional stiffness to the inherent, position-independent stiffness of the CO cannot be neglected. Furthermore, a different substrate material can change the vertical van der Waals forces or a bias between tip and sample can lead to additional electrostatic vertical forces and therefore to a change of the stiffness of the CO tip and of the image distortions.

For large tip heights ($z > 4$ Å) the lateral forces show almost no atomic contrast and no contribution of the Pauli repulsion. For all lat-

eral positions, the lateral forces tilt the CO towards the center of the nearest ring in the FFPB molecule. The tilt leads to a larger appearance of molecules and rings. For smaller tip heights, the tilt of the CO leads not only to the larger appearance of molecules in AFM images but also to a sharper appearance of the bonds, which we will discuss next. This lateral sharpening of the bonds is commonly observed in AFM measurements with CO terminated tips on molecules.[1–10] At small tip heights, approximately when the maximal short range force is reached, the intramolecular bonds appear as sharp lines with a full width of half maximum (FWHM) much smaller than the charge density.[6,30] In Fig. 4, frequency shift linescans above the outer H- and F-ring are shown for different scan heights for the experiment and computations. Note that van der Waals and electrostatic interactions between tip and substrate lead to a height dependent background in the experimental frequency shift curves in Fig. 4(a) and (b). In the computations [Fig. 4(c) and (d)], the sharpening of the bonds can be seen very clearly. With decreasing tip height the FWHM of the peaks becomes smaller. The line shapes deviate more and more from the frequency shifts with a fixed CO (grey dashed lines). Directly above the bonds the Pauli repulsion has its maximum. Above the bond it is energetically more favorable for the CO to tilt away from the bond. As a result the images are locally compressed in these regions and thus the FWHM decreases. This apparent sharpening of bonds is a result of the Pauli repulsion in interplay with the van der Waals interaction. Also the elongated shape of the triple bonds in ethynylene units perpendicular to the direction of the bond in AFM images [Fig. 3(c)] is a result of this intricate interplay. This characteristic distortion of triple bonds has also been experimentally observed in a recent study using CO-terminated tips[8] and is also apparent in the case of FFPB [Fig. 1(b)]. It is important to note that the sharpening is not a dynamic effect and does not originate from the oscillating or scanning motion of the tip. The sharpening can be fully reproduced by the static calculations and is a result of the different tilt angles

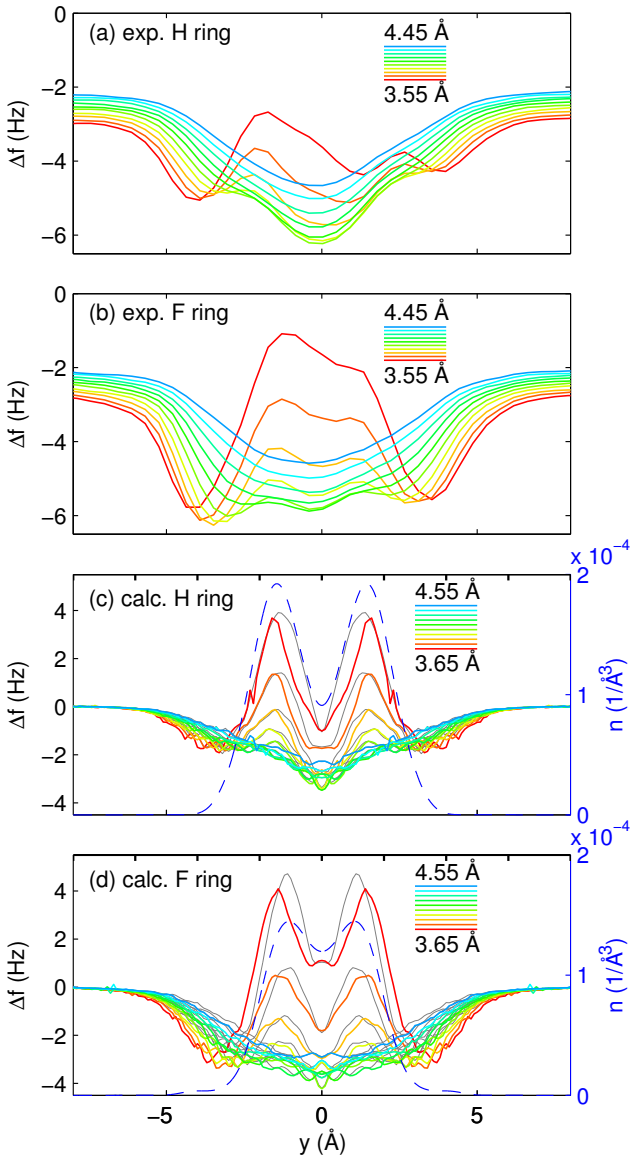

Figure 4: Measured frequency shift Δf linescans through (a) the H-ring and (b) the F-ring as indicated by the arrows in Fig. 1(a) and as a function of the lateral position y. The height spacing between the lines is 0.1 Å. The calculated frequency shift Δf linescans through (c) H-ring and (d) the F-ring with (colored solid lines) and without (thin grey lines) relaxing the tip geometry. Also given is the calculated charge density (dashed blue line) through both rings at height $z = 3.61$ Å.

of the CO molecule at the different lateral tip positions. Lastly, in the center of the rings a maximum appears for very small tip heights as seen in Fig. 4(d) for $z = 3.65$ Å. In experiment

the tip heights are too large for the maximum to appear. However, it has been observed experimentally elsewhere.[6] The reason for this maximum is that there are no lateral forces at this point and the CO is confined in the carbon ring and cannot tilt significantly in any direction due to the surrounding ring of large electron density.

The image distortions of a FFPB molecule in AFM with a CO-terminated tip were studied in detail. We observed experimentally that the fluorinated rings appear with smaller diameter than the hydrogenated rings. The distortions with respect to the atomic positions of the atoms have two origins: the charge density and the tilt of the CO at the tip. Already in the charge density in a plane above the FFPB molecule the rings exhibit different sizes. In addition the molecules appear distorted because of the tilt of the CO due to attractive van der Waals forces. For small tip heights, the Pauli repulsion and the van der Waals interactions together tilt the CO in such a way that the bonds appear sharpened.

Acknowledgement We acknowledge financial support from the EU projects ARTIST (contract no. 243421) and PAMS (contract no. 610446), the ERC Advanced Grant CEMAS, and the Japan Science and Technology Agency (JST) Precursory Research for Embryonic Science and Technology (PREST) for a project of Molecular Technology and Creation of New Function.

References

(1) Gross, L.; Mohn, F.; Moll, N.; Liljeroth, P.; Meyer, G. *Science* **2009**, *325*, 1110–1114.

(2) Moll, N.; Gross, L.; Mohn, F.; Curioni, A.; Meyer, G. *New J. Phys.* **2010**, *12*, 125020.

(3) Neu, M.; Moll, N.; Gross, L.; Meyer, G.; Giessibl, F. J.; Repp, J. *Phys. Rev. B* **2014**, *89*, 205407.

(4) Boneschanscher, M. P.; Hämäläinen, S. K.; Liljeroth, P.; Swart, I. *ACS Nano* **2014**, *8*, 3006–3014.

(5) Guillermet, O.; Gauthier, S.; Joachim, C.; de Mendoza, P.; Lauterbach, T.; Echavarren, A. *Chem. Phys. Lett.* **2011**, *511*, 482–485.

(6) Gross, L.; Mohn, F.; Moll, N.; Schuler, B.; Criado, A.; Guitián, E.; Peña, D.; Gourdon, A.; Meyer, G. *Science* **2012**, *337*, 1326–1329.

(7) Pavliček, N.; Fleury, B.; Neu, M.; Niedenführ, J.; Herranz-Lancho, C.; Ruben, M.; Repp, J. *Phys. Rev. Lett.* **2012**, *108*, 086101.

(8) Oteyza, D. G. d.; Gorman, P.; Chen, Y.-C.; Wickenburg, S.; Riss, A.; Mowbray, D. J.; Etkin, G.; Pedramrazi, Z.; Tsai, H.-Z.; Rubio, A.; Crommie, M. F.; Fischer, F. R. *Science* **2013**, *340*, 1434–1437.

(9) Schuler, B.; Liu, W.; Tkatchenko, A.; Moll, N.; Meyer, G.; Mistry, A.; Fox, D.; Gross, L. *Phys. Rev. Lett.* **2013**, *111*, 106103.

(10) Zhang, J.; Chen, P.; Yuan, B.; Ji, W.; Cheng, Z.; Qiu, X. *Science* **2013**, 1242603.

(11) Matsuo, D.; Yang, X.; Hamada, A.; Morimoto, K.; Kato, T.; Yahiro, M.; Adachi, C.; Orita, A.; Otera, J. *Chem. Lett.* **2010**, *39*, 1300–1302.

(12) Kawai, S.; Sadeghi, A.; Feng, X.; Lifen, P.; Pawlak, R.; Glatzel, T.; Willand, A.; Orita, A.; Otera, J.; Goedecker, S.; Meyer, E. *ACS Nano* **2013**, *7*, 9098–9105.

(13) Hohenberg, P.; Kohn, W. *Phys. Rev.* **1964**, *136*, B864–B871.

(14) Blum, V.; Gehrke, R.; Hanke, F.; Havu, P.; Havu, V.; Ren, X.; Reuter, K.; Scheffler, M. *Comp. Phys. Comm.* **2009**, *180*, 2175–2196.

(15) Perdew, J. P.; Burke, K.; Ernzerhof, M. *Phys. Rev. Lett.* **1996**, *77*, 3865–3868.

(16) Tkatchenko, A.; Scheffler, M. *Phys. Rev. Lett.* **2009**, *102*, 073005.

(17) Ruiz, V. G.; Liu, W.; Zojer, E.; Scheffler, M.; Tkatchenko, A. *Phys. Rev. Lett.* **2012**, *108*, 146103.

(18) Zhang, G.-X.; Tkatchenko, A.; Paier, J.; Appel, H.; Scheffler, M. *Phys. Rev. Lett.* **2011**, *107*, 245501.

(19) Giessibl, F. J. *Appl. Phys. Lett.* **1998**, *73*, 3956–3958.

(20) Albrecht, T. R.; Grütter, P.; Horne, D.; Rugar, D. *J. Appl. Phys.* **1991**, *69*, 668–673.

(21) Mohn, F.; Schuler, B.; Gross, L.; Meyer, G. *Appl. Phys. Lett.* **2013**, *102*, 073109–073109–4.

(22) Mohn, F.; Gross, L.; Meyer, G. *Appl. Phys. Lett.* **2011**, *99*, 053106.

(23) Mohn, F.; Gross, L.; Moll, N.; Meyer, G. *Nat. Nano.* **2012**, *7*, 227–231.

(24) Schuler, B.; Liu, S.-X.; Geng, Y.; Decurtins, S.; Meyer, G.; Gross, L. *Nano Lett.* **2014**, *14*, 3342–3346.

(25) Weymouth, A. J.; Hofmann, T.; Giessibl, F. J. *Science* **2014**, *343*, 1120–1122.

(26) Moll, N.; Gross, L.; Mohn, F.; Curioni, A.; Meyer, G. *New J. Phys.* **2012**, *14*, 083023.

(27) Ternes, M.; Lutz, C. P.; Hirjibehedin, C. F.; Giessibl, F. J.; Heinrich, A. J. *Science* **2008**, *319*, 1066–1069.

(28) Schneiderbauer, M.; Emmrich, M.; Weymouth, A. J.; Giessibl, F. J. *Phys. Rev. Lett.* **2014**, *112*, 166102.

(29) Schwarz, A.; Köhler, A.; Grenz, J.; Wiesendanger, R. *Appl. Phys. Lett.* **2014**, *105*, 011606.

(30) Hapala, P.; Kichin, G.; Wagner, C.; Tautz, F. S.; Temirov, R.; Jelínek, P. *Phys. Rev. B* **2014**, *90*, 085421.